Transition From Periodicity to Chaos in a PWM-Controlled Buck Converter with ZAD strategy

Fabiola Angulo

Universidad Nacional de Colombia

Cra 27 No. 64-60

Manizales (Colombia)

E-mail: fangulo@nevado.manizales.unal.edu.co

Enric Fossas

Technical University of Catalonia

Advanced Control of Energy Systems

Institute of Industrial and Control Engineering

Avda. Diagonal 647, pl 11

08027 Barcelona (Spain)

E-mail: enric.fossas@upc.es

Gerard Olivar

Technical University of Catalonia

Advanced Control of Energy Systems

EPSEVG and FME

Avda. Victor Balaguer, s/n

08800 Vilanova i la Geltrú (Spain)

E-mail: gerard@mat.upc.es

Abstract The transition from periodicity to chaos in a DC-DC Buck power converter is studied in this paper. The converter is controlled through a direct Pulse Width Modulation (PWM) in order to regulate the error dynamics at zero. Results show robustness with low output error and a fixed switching frequency. Furthermore, some rich dynamics appear as the constant associated with the first order error dynamics decreases. Finally, a transition from periodicity to chaos is observed. This paper describes this transition and the bifurcations in the converter. Chaos appears in the system with a stretching and folding mechanism. It can be observed in the one-dimensional Poincaré map of the inductor current. This Poincaré map converges to a *tent map* with the variation of the system parameter k_s.

1 Introduction

Immediately following Lorenz's chaos discovery in 1960's, the scientific community has been interested in describing, and classifying, all routes to chaos. These new routes appear more often in modelling real phenomena rather than in theoretical dynamical systems. This paper describes the transition from periodicity to chaos in a DC-DC buck power converter controlled by a new strategy. Chaos appears in the system with a stretching and folding mechanism which can be observed in the one-dimensional Poincaré map of the inductor current. This Poincaré map converges to a *tent map* with the variation of the system parameter k_s.

DC-DC buck converters decrease a source voltage E. They can be modelled as continuous linear control systems. However, the physical system is a Variable Structure System due a discontinuous control action. This causes abrupt topological changes in the circuit. A detailed introduction to power converters can be found in [Severns & Bloom, 1985]. The control action, usually designed from a continuous time model, is implemented through Pulse Width Modulation. In spite of being linear, chaos appears in DC-DC buck power converters, even when controlled by very simple control actions, such as when a duty cycle occurs from modulating the output voltage by a sawtooth ramp ([Deane & Hamill, 1990], [Fossas & Olivar, 1996], [Olivar, 1997]). Nonlinear phenomena in power electronics (including bifurcations and chaos) can be found in [Banerjee & Verghese, 2001]. Chaotic bands as a final state has been found in many DC-DC converters under different control schemes. In [Chakrabarty *et al.*, 1996], [Yuan *et al.*, 1998], and [Fossas & Olivar, 1996] they are found in a PWM-controlled Buck converter with a modulating sawtooth ramp after smooth period-doubling bifurcations and non-smooth border-collision bifurcations. In [Deane, 1992], [Chan & Tse, 1997], [Tse, 1994] and [Banerjee & Chakrabarty, 1998] chaotic bands are found in current-programmed Boost converters, with and without discontinuous conduction mode. Also, chaotic bands are obtained in [Tse & Chan, 1995] in a current-mode controlled Cuk converter. A boost converter with PWM and voltage control was studied in [El Aroudi *et al.*, 1999]. Chaotic bands were also obtained after smooth Hopf bifurcations. The phenomena of merging bands is also present in the aforementioned studies, but period-doubling bands were not observed. Instead, in the novel and promising ZAD strategy which presented here, the phenomena of doubling bands is observed in a Buck converter.

There are several possible PWM implementations, such as leading, trailing and centered pulse. The third, in turn, can be updated once or twice. The control action considered here, Zero Average Dynamics (ZAD) first proposed in [Fossas *et al.*, 2001], involves a direct design of the duty cycle and is implemented in a single, updated centered PWM. For purposes of robustness, a linear combination of the error and its derivative is considered for the output as in [Bilalovic *et al.*, 1983], [Venkataraman *et al.*, 1985], and [Carpita *et al.*, 1988]. ZAD strategy and its application to power converters are extensively reported in [Fossas *et al.*, 2001], [Ramos *et al.*, 2003], [Ramos et al, 2002(a)], and [Ramos et al, 2002(b)]. The error dynamics time constant appears as a bifurcation parameter. As it varies, a very rich dynamics is observed in the controlled system. It has been reported in [Angulo & Fossas, 2003] that although the system is regulating in a wide region of the parameter space, the current waveform seems to be chaotic in a significant interval.

Thus, from a circuit design viewpoint, it is well worth determining which regions of the parameter space should be avoided. From a mathematical viewpoint, it is interesting to note which kind of bifurcations appear, especially if they are non-smooth and to determine the specific route to chaos.

The paper is structured as follows. Section 2 is a brief introduction to the dynamical system which results from the modelling of the DC-DC Buck converter and its control. Section 3 is devoted to the dynamical system behavior when key parameters are varied in a convenient range. One-dimensional and two-dimensional bifurcation diagrams are described. Also, successive bifurcations are analyzed through to the appearance of the chaos transition. An approximation and a Poincaré map are used in Sec. 4 to show that a slow transition follows the map from periodicity to a chaotic *tent map*. Also chaotic attractors are analyzed after their appearance in post-transition. Sec. 5 describes conclusions and future work.

2 State Space Modelling

Figure 1 shows the blocks diagram of a DC-DC power converter. The signal reference is x_{1ref} and corresponds to the required voltage in the load. If this signal is constant, the system acts as a DC-DC converter. If the signal is sinusoidal, then the system works as a DC-AC converter. In this paper x_{1ref} is assumed constant. The converter is always a step down (or Buck) converter, reducing the DC source voltage to a lower load voltage.

The circuit can be modelled as a linear switching system, such that

$$\begin{pmatrix} \dot{v} \\ \dot{i} \end{pmatrix} = \begin{pmatrix} -\frac{1}{RC} & \frac{1}{C} \\ -\frac{1}{L} & 0 \end{pmatrix} \begin{pmatrix} v \\ i \end{pmatrix} + \begin{pmatrix} 0 \\ \frac{E}{L} \end{pmatrix} u \tag{1}$$

The state variables are the voltage v in the capacitor and the current i in the inductor. Variable $u \in \{-1, 1\}$ is discrete and controls the position of the switches 1 and 2 in Fig. 1. They effect a voltage source of magnitude $+E$ or $-E$. The parameter values are $R = 20\Omega$, $C = 40\mu$F, L=2mH and E=40V. The sampling period is $T_c = 50\mu s$. To obtain dimensionless variables and parameters [Fossas & Zinober, 2001] we apply the following change of variables: $x_1 = v/E$, $x_2 = \frac{1}{E}\sqrt{\frac{L}{C}}i$ and $t = \tau/\sqrt{LC}$, thus $\gamma = \frac{1}{R}\sqrt{\frac{L}{C}}$ and the sampling period is $T = T_c/\sqrt{LC}$ =0.1767. Note that with this change, there are an infinite number of combinations of physical parameters which lead to the same dimensionless parameters.

Then the system equations become

$$\begin{pmatrix} \dot{x}_1 \\ \dot{x}_2 \end{pmatrix} = \begin{pmatrix} -\gamma & 1 \\ -1 & 0 \end{pmatrix} \begin{pmatrix} x_1 \\ x_2 \end{pmatrix} + \begin{pmatrix} 0 \\ 1 \end{pmatrix} u \tag{2}$$

where γ=0.35. With this change, the dimensionless parameters associated to the systems are γ, k_s, x_{1ref} and T.

This system will be controlled with PWM in order to achieve a zero-mean $s(\mathbf{x})$ in every T-cycle such that

$$s(\mathbf{x}) = (x_1 - x_{1ref}) + k_s(\dot{x}_1 - \dot{x}_{1ref}) \tag{3}$$

where x_1 is the variable to be controlled and x_{1ref} is the reference signal. Here k_s is the time constant associated with the first order dynamics given by the surface and which corresponds to the desired error dynamics. This also guarantees that the output x_1 follows the reference x_{1ref}.

When the system works implements centered PWM, the injected control signal can be defined through Eq. (4) such that

$$u = \left\{ \begin{array}{cl} 1 & \text{if } kT \le t \le kT + l/2 \\ -1 & \text{if } kT + l/2 < t < kT + (T - l/2) \\ 1 & \text{if } kT + (T - l/2) \le t \le kT + T \end{array} \right\} \tag{4}$$

where the switching time l (which can vary from cycle to cycle and is the time duration when the source is in $+E$) is computed in order to maintain

$$\int_{kT}^{(k+1)T} s(\mathbf{x}(t))dt = 0 \tag{5}$$

By enforcing this equality, we try to obtain zero-mean error dynamics in each sampling cycle to achieve a fixed frequency of commutation. Computing the exact switching time l in each iteration requires solving a transcendental equation, which is significantly burdensome. In [Biel *et al.*, 2002] and [Angulo & Fossas, 2003], an approximation of the switching time was found to be

$$l = \frac{2s(0) + T\dot{s}_2}{\dot{s}_2 - \dot{s}_1} \tag{6}$$

where $s(0)$ is the value of the surface at the sampling instant, and $\dot{s}_1$ and $\dot{s}_2$ are the derivatives in the last and the previous linear piece, respectively. Here, $\dot{s}_2$ can be computed with the same data that is used for $\dot{s}_1$ and changing the sign of excitation u.

For the sake of simplicity, we assume that the pulse sign is positive between kT and $kT + \frac{l}{2}$ the pulse sign is positive, and that the pulse changes to -1 between $kT + \frac{l}{2}$ and $(k+1)T - \frac{l}{2}$. In the last part of the cycle, the pulse returns to 1. Inverting the order in the pulses does not lead to any significant difference [Angulo & Fossas, 2003]. We will refer to the time evaluated at $t = kT$ as the *sampling instant* for any k, and *commutation instant* as the time when the pulse changes from $+1$ to -1 (or from -1 to $+1$). The commutation instants are $t = kT + l/2$ and $t = (k+1)T - l/2$ for any k.

Thus, the state at $t = kT$ ($\mathbf{x}(kT)$) will be the sampling state and the state at $\mathbf{x}(kT + l/2)$ and $\mathbf{x}((k+1)T - l/2)$ will be the switching (or commutation) states. Figure 9 shows all of these states in the state space. It also shows the evolution of a stable orbit. Since this is a linear time invariant system driven by unitary pulses, the solution can be obtained through direct integration and yields

$$\mathbf{x}\left((k+1)\,T\right) = e^{\mathbf{A}T}\mathbf{x}\left(kT\right) + \left(e^{\mathbf{A}(T-l/2)} + \mathbf{I}\right)\mathbf{A}^{-1}\left(e^{\mathbf{A}l/2} - \mathbf{I}\right)\mathbf{b} - e^{\mathbf{A}l/2}\mathbf{A}^{-1}\left(e^{\mathbf{A}(T-l)} - \mathbf{I}\right)\mathbf{b} \tag{7}$$

In all of the subsequent analysis we will assume that the feeding scheme is $+1$, -1, $+1$. The sign changes are performed internally. In [Angulo & Fossas, 2003] the existence of a threshold value for the time constant associated with the error dynamics was reported. Below the threshold, the system becomes unstable and a transition to chaos is obtained. In the report, the stability limit was studied via linearization and Floquet

and Lyapounov exponents. However, when the system makes the transition to chaos no qualitative or quantitative analysis was performed.

The equation for the switching time, as a function of the states is given by

$$l = \frac{2 - 2k_s\gamma + Tk_s\gamma^2 - \gamma T - Tk_s}{-2k_s}x_1(0) + \frac{2k_s + T - k_s\gamma T}{-2k_s}x_2(0) - \frac{2x_{1ref}}{-2k_s} - \frac{Tk_s}{-2k_s} \tag{8}$$

Limits of system behavior are given at $l = 0$ and $l = T$ (saturation of the switching time) according to the Eq. (9). These boundaries are shown in Fig. 2 will be denoted as P and Q, respectively.

$$0 \leq \frac{2 - 2k_s\gamma + Tk_s\gamma^2 - \gamma T - Tk_s}{-2k_s}x_1(0) + \frac{2k_s + T - k_s\gamma T}{-2k_s}x_2(0) - \frac{2x_{1ref}}{-2k_s} - \frac{Tk_s}{-2k_s} \leq T \tag{9}$$

Between these boundaries the system dynamics follows Eqs. (7) and (8). Outside this region the system follows the following dynamics:

$$\mathbf{x}(k+1)T = \begin{cases} e^{\mathbf{A}T}\mathbf{x}(kT) + \mathbf{A}^{-1}(e^{\mathbf{A}T} - \mathbf{I})\mathbf{b}, & \text{if } l \geq T \\ e^{\mathbf{A}T}\mathbf{x}(kT) - \mathbf{A}^{-1}(e^{\mathbf{A}T} - \mathbf{I})\mathbf{b}, & \text{if } l \leq 0 \end{cases} \tag{10}$$

Several numerical simulations have shown that when the value of k_s is below the stability threshold, the system is still regulating. Thus, the output does not change significantly and allows for some critical simplifications with respect to state x_1.

When the switching time is between 0 and T, two switching points exist and correspond to states $\mathbf{x}(l/2)$ and $\mathbf{x}(T - l/2)$. We have computed all possible switching points (curves X(l/2) and X(T-l/2)) in the state space as follows: (1) We assume that the system is regulated. That is, we assume $x_1(0)$ =0.7996, which is the stationary value for a reference signal x_{1ref}=0.8. (2) We take any $l \in [0, T]$ and we substitute it in Eq. (8) to obtain the value of $x_2(0)$. (3) Once $x_2(0)$ has been evaluated, we have all the required information to solve the state equations (Eq. (2) for $t = l/2$ and $t = T - l/2$) and (4) The border curves corresponding to the switching states can be computed and plotted, as is shown in Fig. 3.

It should be noted that for l=0, the switching curve corresponding to X(l/2) collides with the upper limit due to the initial condition $\mathbf{x}(0)$. Curves X(l/2) and X(T-l/2) meet at $l = T$. When the value of k_s decreases, the symmetry of the curves is lost.

Another critical curve is that of the image of the curve Q (obtained from Eq. (7) and taking initial conditions on Q). This curve image will henceforth be denoted by R. Any initial condition below the curve

Q maps below R. (see Fig. 3).

This division of the state space effects the easier analysis of the transition to chaos and will shown in the following sections.

3 Bifurcations

For T=0.1767, γ=0.35, x_{1ref}=0.8, and k_s=4.5, simulations show that the stationary dynamics is an asymptotically stable T-periodic orbit. If we reduce the value of k_s, and fix the remaining parameters, then a bifurcation occurs near k_s=3.25. In [Angulo & Fossas, 2003] a detailed study can be found including analytical and numerical techniques to precisely compute this bifurcation value.

By reducing k_s slightly further (of order of 0.001), the system shows $2T$-periodic stable orbits with no saturation cycles. If the value of k_s is reduced even further, another class of $2T$-periodic orbits with one saturation cycle and one non-saturated cycle is obtained. And, a smooth period-doubling and a corner collision bifurcation occurs. As the parameter is still further decreased beyond a certain value, the $4T$-periodic orbits become 4-chaotic bands in another non-smooth transition. Bifurcations of stable mT-periodic orbits (for a certain m) to m-band chaos has been observed in other systems and specifically in other DC-DC converters ([Banerjee, 1997], [Olivar, 1997]), and are also predicted by the existing bifurcation theory of non-smooth systems [Banerjee & Grebogi, 1999]. Further computations show that this 4-band splits into an 8-band and the process continues *at infinitum* (see Fig. 21). To our knowledge, this is the first time that a (non-smooth) period doubling band process has been observed. The details of this phenomenon will be reported in a future paper. The width of these bands widens as the parameter k_s decreases and the phenomenon is practically unobservable in the beginning of the band-merging process. Finally, the sequence of merging bands crises ([Ott, 1993], [Banerjee & Verghese, 2001]) ends in a chaotic 1-band attractor (see Figs. 6, 7, 8). Section 4 gives intuitive reasoning for why these bands are created.

Simulations in light of other parameters show that the value of k_s in the first bifurcation lightly changes as the parameter x_{1ref} is varied, but the variations are not significant [Angulo & Fossas, 2003]. Similar one-dimensional bifurcation diagrams (with k_s as bifurcation parameter) are obtained for different values of x_{1ref}, such is the reason for not taking into account in the following analysis. We will assume x_{1ref}=0.8.

Another bifurcation parameter is the sampling time T. Figure 4 shows a two-dimensional bifurcation diagram with T and k_s as bifurcation parameters.

The colors corresponding to the diagram are as follows: T-periodic stable orbits are plotted with cyan, yellow corresponds to $2T$-periodic stable orbits, $3T$-periodic stable orbits are plotted in green, blue corresponds to 4-band stable chaos, red to 8-band stable chaos, black to 16-band stable chaos, and other stable chaotic attractors are plotted in magenta. In this plot γ=0.35. Note that high values of the period imply a higher ripple in the output voltage, causing the system to lose its regulation capacity. Thus we will not vary T significantly.

Fig. 5 shows a two-dimensional bifurcation diagram of the system under variation of parameters k_s and γ. In it, a global picture of how the stable periodic orbits and the chaotic bands are distributed is given. Here, k_s is the parameter associated with the sliding surface and γ is the unique parameter associated to the circuit's physical components. It can be observed that the transition to chaos is very fast, and the 4-chaotic bands evolve in a very small range of k_s. Also, as γ decreases the transition to chaos is faster.

In the following, we perform a detailed study of the successive bifurcations occurring in the system. The analysis corresponds to T=0.1767, γ=0.35, x_{1ref}=0.8, and with varying k_s.

The first bifurcation is detailed in [Angulo & Fossas, 2003]. It is of flip type since one of the Floquet multipliers pass through -1 [Kuznetsov, 1998]. We will study the successive bifurcations and the transition to chaos. Figures 6 through 8 show one-dimensional bifurcation diagrams with k_s as the bifurcation parameter and with the output voltage, the inductor current and the duty cycle as bifurcation states.

Figure 6 shows that, although the system enters the chaotic zone, the circuit is still regulated (note that the voltage scale is very tight). The corresponding voltage variable is very near to the reference signal x_{1ref}=0.8 and it held almost constant, which will allow some useful approximations and simplifications.

3.1 First bifurcation

A standard linear analysis allows the conclusion that the first bifurcation, as was previously stated, is of flip type because one of the Floquet multipliers of the T-periodic orbit passes through -1. Figure 9 shows the evolution of the T-periodic stable orbit for k_s=4.5. This orbit will bifurcate into a stable $2T$-periodic orbit and an unstable T-periodic orbit for $k_s \approx 3.25$ (shown in Fig. 10).

Let us consider the discrete-time Poincaré map P_T corresponding to Eqs. (7), (10). A stable $2T$-periodic orbit in the continuous system corresponds to two 2-periodic points in the state space for this T-sampled Poincaré map P_T. One of the orbits is closer to the curve Q (point D in Fig. 10) and the other one (point A in Fig. 10) is close to curve R. Also, four new switching points are generated near the two switching points of the previous T-periodic stable orbit. One (B) is moved to the right and one (E) is to the left, both on the curve X(l/2). The other two points are on the curve X(T-l/2). One is to the right (C) and the other is to the left (F) of the corresponding point of the previous T-periodic stable orbit.

The fact that one switching point is on the right and the other is on the left implies a lower and a higher value for the corresponding switching times. This is because the upper point approaches curve P (which corresponds to $l = 0$) and the lower point approaches curve Q (which corresponds to $l = T$). As the parameter k_s decreases, two of the points (E and F in Figs. 10 and 11) will approach the corner of the curves X(l/2) and X(T-l/2), which is obtained for $l = T$.

Following this process, for k_s=3.2425, the stable $2T$-periodic orbit is plotted in Fig. 11.

The next bifurcation corresponds no longer to flip type but to corner collision type ([di Bernardo *et al.*, 2001], [Yuan *et al.*, 1998]).

3.2 Second bifurcation

In the state space, as k_s is varied, the stable 2-periodic orbit approaches the boundary Q. And, for a specified parameter value, this discrete-time orbit collides with the boundary in a corner collision bifurcation (or transition). In this bifurcation, the number of equilibrium points does not change but the evolution of the orbits in the state space is different (shown in Fig. 12).

A 2-periodic orbit of the T-sampled Poincaré map P_T is a 1-periodic orbit (or fixed point) of the map P_T^2. Table 1 shows the characteristic multipliers of the fixed point of P_T^2, as k_s is lightly varied near the bifurcation value. Before the bifurcation, (k_s=3.2425) we observe two non-saturated cycles. After the transition, we have a 2-periodic orbit with one saturated cycle and one non-saturated cycle. We can observe a discontinuity in the Jacobian at the periodic orbit, since the eigenvalues of the linearized system change suddenly.

In the approximate range $k_s \in [2.995, 3.242]$, there are still 2-periodic orbits with one saturated cycle

and one non-saturated cycle. In the phase space, P_T maps one of the two points of the periodic orbit (the one which is below the border Q) to the other point (which is near and below R), without any commutation point in the curves X(l/2) or X(T-l/2). Then, a non-saturated cycle follows with switching time $0 < l < T$, and the point is mapped again by P_T near the border Q.

Again, with a slight variation of the bifurcation parameter, one of the eigenvalues passes through -1 in another flip bifurcation, which occurs near approximately k_s=2.998.

3.3 Third bifurcation

Effectively, the third bifurcation is of flip type. This can be confirmed by computing the eigenvalues of P_T^2 (the second iteration of P_T), at the periodic orbit. Table 2 shows these eigenvalues near the bifurcation value. After the bifurcation, the stability of the 2-periodic orbits is changed and 4-periodic stable orbits appear.

One of the two points (D in Fig. 12) corresponding to the former 2-periodic orbit splits into two points (D and H in Fig. 13) but both below the border Q. Thus, they give rise to saturated cycles, and their images by P_T are situated below R. They are very close to one another, and this implies that the values of the corresponding switching times are also very close (shown in Fig. 13). This process of approaching points will end in a band creation process, as will be shown later (see Fig. 22).

As was previously stated in the presentation of the 2-dimensional bifurcation diagrams, 4-bands appear in a very narrow range of the bifurcation parameter k_s, and thus the 8-bands appear almost immediately.

3.4 Fourth bifurcation and the beginning of chaos

For a certain bifurcation value of k_s between 2.5 and 3 a small region in the border Q and its image by P_T act as accumulation regions of points, and the chaotic period 4 bands appear. This may be due to a corner collision bifurcation of the type 2^n*-periodic stable orbit to chaotic* 2^n*-band* ([Banerjee, 1997],[Olivar, 1997]). As such, chaos is introduced to the system.

It should be noted that for this value of the parameter (and below), the simplification in the analysis treating X(l/2) and X(T-l/2) as curves instead of regions leads to a loss accuracy; this simplification is merely an approximation because the commutation points should be situated in the curves. Other

computations (not included in this paper) show that as the parameter value is further decreased, successively merging band crises appear, resulting in a 1-band chaos.

Also note that the smooth and nonsmooth bifurcations found in this section are not specific to the choice of parameter values. As can be observed from the two-dimensional bifurcation diagrams (see Fig. 5), varying parameters k_s or γ results in the same bifurcations, although they occur in different ranges.

4 Transition to Chaos: Another Viewpoint

In this section we will emphasize the 1-dimensional Poincaré map of the current variable x_2 as the main tool to describe the transition of periodicity to chaotic motion.

Since the system is regulated for a wide range of k_s, the Poincaré map is very close to 1-dimensional (note that the value of the voltage is almost constant). Thus we assume that $x_1(0) = 0.7996 \approx x_{1ref}$, which simplifies the solutions.

The procedure to compute the 1-dimensional Poincaré map P_T is divided in two parts: one, when the switching time is less than T (no saturation); and two, when there is a saturation cycle.

For the first part, k_s is fixed and we take a value of $l \in [0, T]$. With $l \in [0, T]$ and the state $x_1(0)$=0.7996, we apply Eq. (8) to compute $x_2(0)$. Using $x_1(0)$, $x_2(0)$ and $t \in [0, T]$ we apply the Poincaré map in Eq. (7). It is observed that any point near the curve P (x_2 ≈0.44) is mapped to an image far below curve Q (x_2 ≈0.13). Thus, the next cycle must be saturated, without any possibility of returning to the initial point. That is, the system tends to remain inside the region between the border curves Q and R. Thus, we consider initial values $(x_1(0), x_2(0))$ between curves R and Q. Hence, $l \in [d_1, T]$ for a certain l_1.

For the second part, we have a saturated cycle. Thus, we first generate the points $x(f)$ which are mapped below the curve Q (these are the points which will have a saturated cycle). We can then use Eq. (10) to compute the image of these points.

For generating the diagram $x_2(k+1)$ vs $x_2(k)$, we compute one iteration of the 1-dimensional Poincaré map. Curve x(0) in Fig. 14 is mapped on curve x(f).

Analitically, the expression of the 1-dimensional Poincaré map can be obtained through Eqs. (11) and (12).

If $0 < l < T$,

$$\begin{aligned} x_2(k+1) &= e_{21}(T)x_1(k) + e_{22}(T)x_2(k) - e_{21}(T) + 2e_{21}(T - l/2) - \gamma e_{22}(T) + 2\gamma e_{22}(T - l/2) \\ &\quad -2e_{21}(l/2) - 2\gamma e_{22}(l/2) + \gamma \end{aligned} \tag{11}$$

$$l = \frac{2 - 2k_s\gamma + Tk_s\gamma^2 - \gamma T - Tk_s}{-2k_s}x_1(k) + \frac{2k_s + T - k_s\gamma T}{-2k_s}x_2(k) - \frac{2x_{1ref}}{-2k_s} + \frac{T}{2} \tag{12}$$

where e_{21} and e_{22} correspond to the terms $\{2,1\}$ and $\{2,2\}$ of the system state transition matrix and $x_1(k) = 0.7996$ from the regulation assumption.

If $l > T$,

$$x_2(k+1) = e_{21}(T)x_1(k) + e_{22}(T)x_2(k) - e_{21}(T) - \gamma e_{22}(T) + \gamma \tag{13}$$

We will denote $\mathbf{x}(0)$ as the initial points and $\mathbf{x}(f)$ as the images. Fig. 15 shows the results for $k_s = 4.5$. The images lie almost on the initial points (note the tightness in the voltage scale). A point in the upper region is mapped to the lower region and viceversa. Since the range of values of $\mathbf{x}(f)$ is smaller than that of $\mathbf{x}(0)$ a stretching phenomena appears.

Figure 16 shows the map of $x_2(k+1)$ vs $x_2(k)$. The map clearly shows a stable periodic point (the modulus of the derivative is less than 1). All initial conditions converge to the equilibrium x_2=0.2799 (note that only the initial process is shown).

Further decreasing k_s below 3.24 results in a different behavior. In the image of $\mathbf{x}(0)$, a small segment below Q starts to grow. As parameter k_s is varied further, the segment that grows below Q in the state space gets bigger and bigger, and a map very close to a *tent map* is obtained. This is why the map evolves from periodicity to chaotic motion, as it was previously stated. Figures 17 and 18 show the behavior of the system.

Figure 19 shows the Poincaré map for k_s=0.5 and Fig. 20 shows the behavior of $x_2(k+1)$ vs $x_2(k)$ for the same value of parameter. It can be clearly seen in this figure the effect of decreasing the parameter associated to the sliding surface.

If we expand Eq. (11) in Taylor series and taking into account that Eq. (13) is linear, we obtain, for the aforementioned values, the approximated linear map

$$x_2(k+1) = \begin{cases} 0.0388 + 0.9869x_2(k) & \text{if } x_2(k) \leq 0.264 \\ 0.6416 - 1.2871x_2(k) & \text{if } x_2(k) \geq 0.264 \end{cases} \tag{14}$$

As it can be observed, this corresponds to a tent map. Now we compare the original nonlinear map (11) with the approximated linear map (14). Namely, the Taylor theorem allows to fit the error. For any smooth and finite map $f(x)$ defined on the interval $(a,\ b)$ there exists $c \in [a,b]$ such that for all $h \in (a,\ b)$

$$f\left(h\right) = f\left(c\right) + \frac{f'\left(c\right)}{1!}(h-c) + \cdots \frac{f^{n-1}\left(c\right)}{(n-1)!}(h-c)^{n-1} + \epsilon_f$$

for $|\epsilon_f| \leq \left| f^{(n)}(h_1)\frac{(h-c)^n}{n!} \right|$ and $h_1 \in (a,b)$.

In our case, $c = 0.264$ and $|h-c| \leq 0.036$, and thus, the error in the approximated tent map is everywhere less than $0.44e-6$.

Thus, the original nonlinear map is very well approximated by the tent map, yielding a well-known route to chaos (see [Nusse & Yorke, 1997]), which is closely related to the obtained route to chaos in the ZAD buck converter.

4.1 Chaotic attractors

For values of k_s approximately lower than 2.5 chaos is detected in the system. This occurs after the 2^n-periodic stable orbit bifurcates into a chaotic 2^n-band in a non-smooth bifurcation (for $n = 2$). In this subsection we show numerically the evolution of the chaotic attractor as the bifurcation parameter k_s is decreased.

After the period-doubling band process, a band merging sequence follows. Figures 21 - 22 show the merging bands as k_s decreases from 2.5 to 1.

In the merging bands process, the bands join two by two until a one-band chaotic attractor is obtained. Figures 21 - 23 show the evolution of the attractor as k_s is further decreased. Other computations not included in this paper have shown that the number of fingers in the attractor (see Fig. 23) is closely related to the frequency of saturated cycles in the orbits.

As k_s is still further decreased, the chaotic attractor collapses and the system behavior is again periodic. That occurs since the trajectories tend to an equilibrium point in the state space. This is shown in the 2-dimensional bifurcation diagram in Fig. 5.

The equilibrium point corresponds to $x_1 = -1$, characterized by a saturated cycle. The value of the source is always -1 and the capacitor is loaded with this value. Regulation is also lost. A so low value of

k_s makes that the sliding surface cannot reach its desired objective.

5 Conclusions and Further Research

Several smooth and non-smooth bifurcations have been studied with detail in a PWM-controlled buck converter with ZAD strategy. A simplification due to the regulation characteristic of the converter allows some analytical work. Also numerical computations can be made faster.

Flip bifurcations and corner collision bifurcations have been clearly detected. For a specific n, the 2^n-periodic stable orbit bifurcates to a chaotic 2^n-band, and a period-doubling band sequence begins. They finally lead to a one-band chaotic attractor after a merging band crises process.

Using the simplification due to the regulation assumption, we have shown that the one-dimensional map corresponding to the current variable tends to a tent-like map. Thus, with this specific control strategy in the buck converter, we have shown that chaos is clearly present.

The evolution of the chaotic attractor for $k_s \in [0.165,\ 1]$ and the analysis of period doubling band process will be analyzed in a future paper.

6 Acknowledgements

The authors gratefully acknowledge support from the European Union (FP5 EU Project SICONOS IST-2001-37172).

References

Angulo F. & Fossas E. [2003] "Control a frecuencia fija para un ondulador con modulador de ancho de pulso centrado," *Reporte interno de investigación Instituto de Organización y Control de Sistemas Industriales*. Universidad Politécnica de Cataluña.

Banerjee S. [1997] "Coexisting Attractors, Chaotic Saddles, and Fractal Basins in a Power Electronic Circuit," *IEEE Trans. on Cir. and Sys.*, Vol. 44, no. 9, pp. 847-849.

Banerjee S. & Chakrabarty K. [1998] "Nonlinear Modeling and Bifurcations in the Boost Converter," *IEEE Trans. on Power Electr.*, Vol. 13, no. 2, pp. 252-260, March 1998.

Banerjee S. & Grebogi C. [1999] "Border collision bifurcations in two-dimensional piecewise smooth maps," *Physical Review E*, vol. 59, no. 4, pp. 4052-4061.

Banerjee S. & Verghese G.C., Eds. [2001] *Nonlinear Phenomena in Power Electronics*, IEEE Press, Piscataway.

Biel D., Fossas E., Ramos R. & Guinjoan F. [2002] "Implementación de controles "pseudo-sliding" en sistemas conmutados," *Congreso Latinoamericano de Control Automático*. Guadalajara, Mexico (in Spanish).

Bilalovic F., Music O., & Sabanovic A., [1983] "Buck converter regulator operating in the sliding mode," *Proceedings VII International PCI*, pp. 331-340.

Carpita M., Marchesoni M., Oberti M. & Puguisi L. [1988] "Power conditioning system using slide mode control," in *Proceedings of the IEEE Power Electronics Specialist Conference*, pp 623-633.

Chakrabarty K., Poddar G. & Banerjee S. [1996] "Bifurcation Behavior of the Buck Converter," *IEEE Trans. on Power Electr.*, vol. 11, no. 3, pp. 439-447, May 1996.

Chan W.C.Y. & Tse C.K. [1997] "Analysis, Simulation and Experimental Study of Chaos in the Buck Converter," *IEEE Power Electronics Specialists Conference*, Vol. II, PESC'90 Records, pp. 491-498, San Antonio TX.

Deane J.H.B. [1992] "Study of Bifurcations in Current-Programmed DC/DC Boost Converters: From Quasi-Periodicity to Period-Doubling," *IEEE Trans. on Circuits and Systems, Part I*, Vol. 44, No. 12, pp. 1129-1142, December 1997.

Deane J.H.B. & Hamill D.C. [1990] "Analysis, Simulation and Experimental Study of Chaos in the Buck Converter," *IEEE Power Electronics Specialists Conference*, Vol. II, PESC'90 Records, pp. 491-498, San Antonio TX.

di Bernardo M., Budd C.J. & Champneys A.R. [2001] "Grazing and Border-Collision in Piecewise Smooth Systems: a unified analytical framework," *Phys. Rev. Lett.* 86, pp. 2553-2556.

El Aroudi A., Benadero L., Toribio E. & Olivar G. [1999] "Hopf Bifurcation and Chaos from Torus Breakdown in a PWM Voltage-Controlled DC-DC Boost Converter," *IEEE Trans. on Cir. and Sys., Part I*, vol. 46, no. 11, pp. 1374-1382, November 1999.

Fossas E. & Olivar G. [1996] "Study of Chaos in the Buck Converter," *IEEE Trans. on Cir. and Syst.*, vol. 43, no. 1, pp. 13-25.

Fossas E. & Zinober A. [2001] "Adaptive tracking control of nonlinear power converters," in *Proceedings IFAC Workshop on Adaptation in Control and Signal Processing.* Connobio. Italia, pp 264-266.

Fossas E., Griñó R. & Biel D. [2001] "Quasi-Sliding Control Based on Pulse Width Modulation, Zero Average and the L_2 norm,", in *Advances in Variable Structure System, Analysis, Integration and Applications.* Edited by X. Yu and J-X. Xu, World Scientific, pp. 335-344.

Kuznetsov Y. A. [1998] *Elements of Applied Bifurcation Theory.* 2nd edition. Springer Verlag. New York, pp 482-488.

Nusse H. E. & Yorke J.A. [1997] *Dynamics: Numerical Explorations.* Springer Verlag. New York, 1997.

Olivar G. [1997] *Chaos in the Buck Converter*, Ph.D.Thesis, Barcelone.

Ott, E. [1993] *Chaos in Dynamical Systems.* Cambridge University Press, Cambridge.

Ramos R., Biel D., Fossas E., & Guinjoan F. [2003] "Fixed-Frequency Quasi-Sliding Control Algorithm: Application to Power Inverters Design by Means of FPGA Implementation," *IEEE Trans. on Power Electronics*, v. 18, no. 1, pp. 344-355.

Ramos R., Biel D., Guinjoan F. and Fossas E. *Distributed control strategy for parallel-connected inverters. sliding mode control approach and FPGA-based implementation.* IEEE 2002 28th Annual Conference of the IECON 2002 (Industrial Electronics Society), vol. 1, November 5 - 8, 2002. pp 111 -116.

Ramos R., Biel D., Guinjoan F. and Fossas E. *Design considerations in sliding-mode controlled parallel-connected inverters.* IEEE International Symposium on Circuits and Systems, 2002. ISCAS 2002. vol. 4, 26-29 May 2002. pp IV-357 -IV-360.

Severns R.P. & Bloom G. [1985] *Modern DC to DC Switch-Mode Power Converter Circuits*, Van Nostrand-Rheinhold, New York.

Sira-Ramírez, H. [1987] "Sliding Motions in Bilinear Switching Networks," *IEEE Trans. Circ. and Syst.-I*, v. 34, no. 8, pp. 919-933.

Tse C.K. [1994] "Flip Bifurcation and Chaos in Three-State Boost Switching Regulators," *IEEE Trans. on Circuits and Systems, Part I*, Vol. 41, No. 1, pp. 16-23, January 1994.

Tse C.K. and Chan W.C.Y. [1995] "Instability and Chaos in a Current-mode Controlled Cuk Converter," *IEEE PESC'95*, pp. 608-613, Atlanta, Georgia, 1995.

Yuan G., Banerjee S., Ott E. & Yorke J.A. [1998] "Border-Collision Bifurcations in the Buck Converter," *IEEE Trans. on Cir. and Sys.*, vol. 45, no. 7, pp. 707-716.

Venkataramanan R. Sabanović A. & Ćuk S., [1985] "Sliding Mode Control of DC-to-DC Converters," *Proceedings IECON 1985*, pp. 251-258.

Table 1: *Characteristic multipliers of P_T^2 at the periodic orbit.*

k_s	2-periodic: non sat. - non sat.	2-periodic: sat. - non sat.
3.2425	0.8974131, 0.9999910	
3.242		0.89815254, -0.99129

Table 2: *Characteristic multipliers of the second iteration of the Poincaré map, P_T^2.*

k_s	λ_1	λ_2
3.0	0.89043	-0.999907
2.998	0.890369	-0.99985
2.997	0.890335	-1.0000237

Figure 1: Scheme of a PWM-controlled power converter.

Figure 2: Region in the state space (shadowed region) where there is not a saturation in the duty cycle.

Figure 3: Different regions in the state space. The region between curves R and Q gives non-saturated cycles. Curve Q maps on R after one (saturated) cycle. The curves X(l/2) and X(T-l/2) are the commutation curves, where the topology changes. They meet at a non-differentiable point for $l = T$.

Figure 4: Two-dimensional bifurcation diagram. k_s and T are the bifurcation parameters. See text for the color codes.

Figure 5: Two-dimensional bifurcation diagram. Bifurcation parameters are k_s and γ. The color codes are the same like in the previous two-dimensional bifurcation diagram.

Figure 6: One-dimensional bifurcation diagram. Voltage vs k_s.

Figure 7: One-dimensional bifurcation diagram. Inductor current vs k_s.

Figure 8: One-dimensional bifurcation diagram. Duty cycle vs k_s.

Figure 9: Evolution of the T-periodic orbit in the state space, k_s=4.5.

Figure 10: Evolution of the stable $2T$-periodic orbit in the state space, k_s=3.2443.

Figure 11: Evolution of the stable $2T$-periodic orbit in the state space, k_s=3.2425.

Figure 12: Evolution of the $2T$-periodic orbit in the phase space, k_s=3.242.

Figure 13: Evolution of the $4T$-periodic orbit in the state space, $k_s = 2.998$.

Figure 14: Global view of the Poincaré map in the 2-dimensional state space. Note the voltage scale in the diagram implying that the map is almost 1-dimensional.

Figure 15: Behavior of the states through the map P_T. k_s=4.5. $x(0)$ is mapped to $x(f)$. All the images are in the region between the curves R and Q, and thus there are no saturated cycles. Consequently, the 1-dimensional Poincaré map is linear (see Fig. 16).

Figure 16: 1-dimensional Poincaré map for the evolution of the current. k_s=4.5. The modulus of the derivative of the fix point is less than 1. Thus it is asymptotically stable.

Figure 17: Behavior of the states in the Poincaré map. k_s=2.8. $x(0)$ is mapped to $x(f)$. There are some images below curve Q and thus some cycles are saturated. Then, the Poincaré map is piecewise-linear (see Fig. 18).

Figure 18: 1-dimensional Poincaré map for the evolution of the current. k_s=2.8. The map is piecewise-linear. The modulus of the derivative of the fix point is larger than 1. Thus it is unstable.

Figure 19: Behavior of the states in the Poincaré map. k_s=0.5. $x(0)$ is mapped to $x(f)$. A large part of the images is below curve Q, which means saturation. The corresponding Poincaré map is piecewise-linear, similar to a chaotic tent-map (see Fig. 20).

Figure 20: 1-dimensional Poincaré map for the evolution of the current, showing tent-map chaotic characteristics. k_s=0.5.

Figure 21: Evolution of the attractor in the period-doubling band process. k_s=2.5.

Figure 22: Evolution of the chaotic attractor, with 4 bands. k_s=1.0.

Figure 23: Evolution of the attractor. k_s=0.165. The observed fingers of the attractor are related to the frequency of saturated cycles.

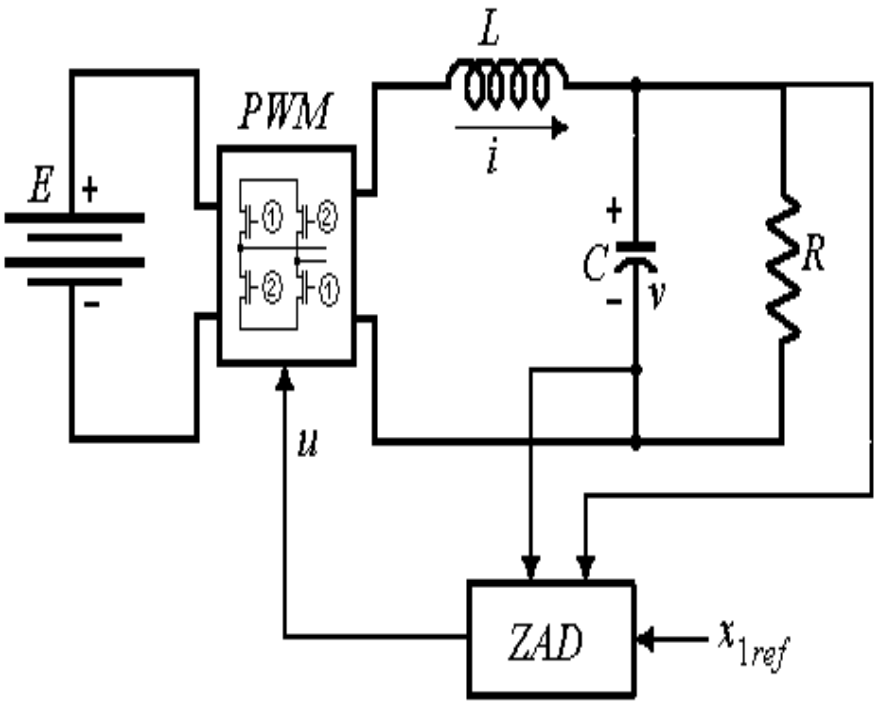

Figure 1: Figure's author: Fabiola Angulo.

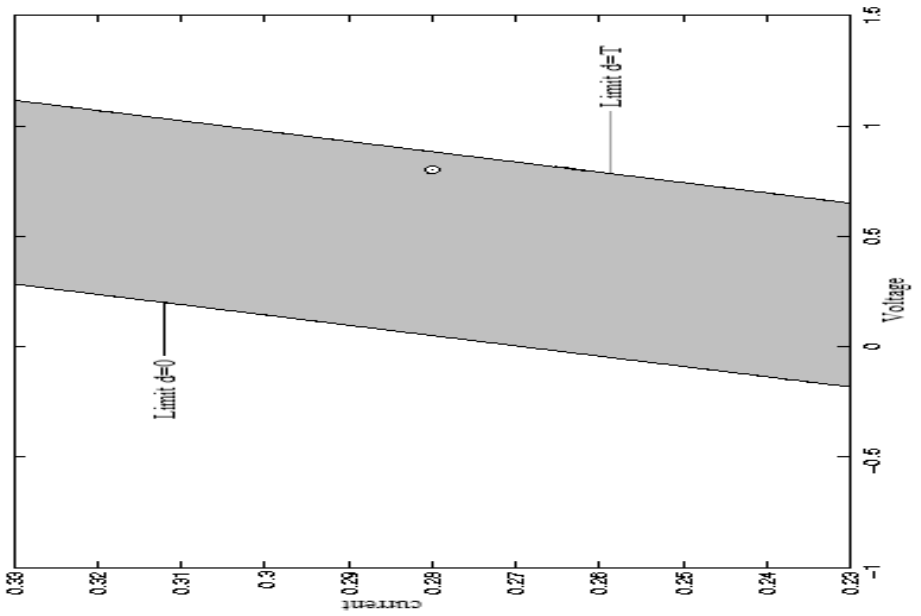

(a) k_s=4.5

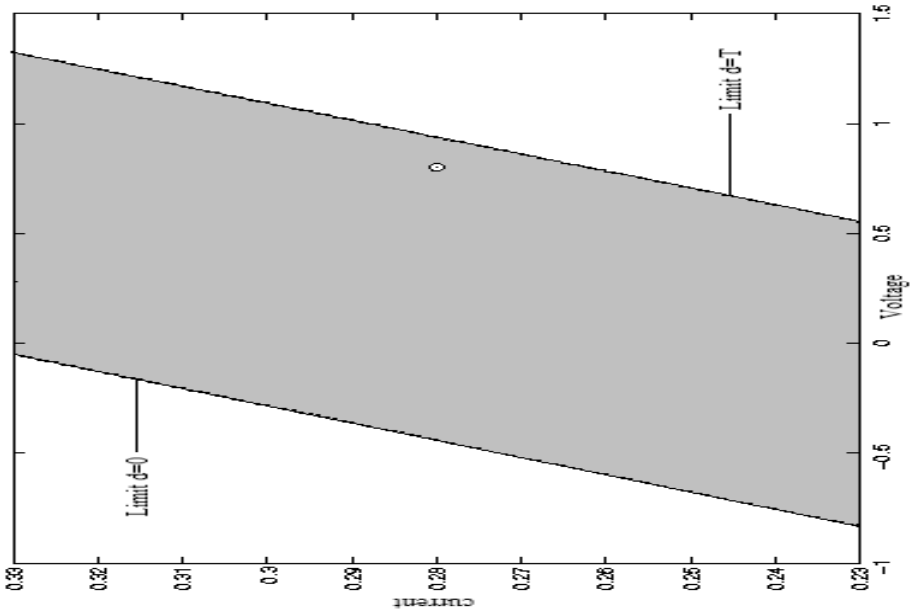

(b) k_s=3.24

Figure 2: Figure's author: Fabiola Angulo.

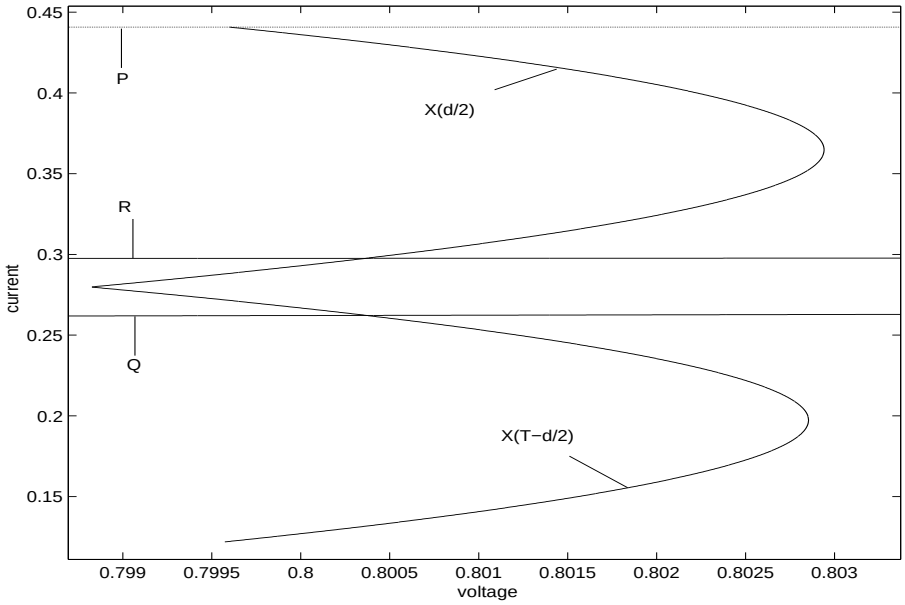

(a) k_s=4.5

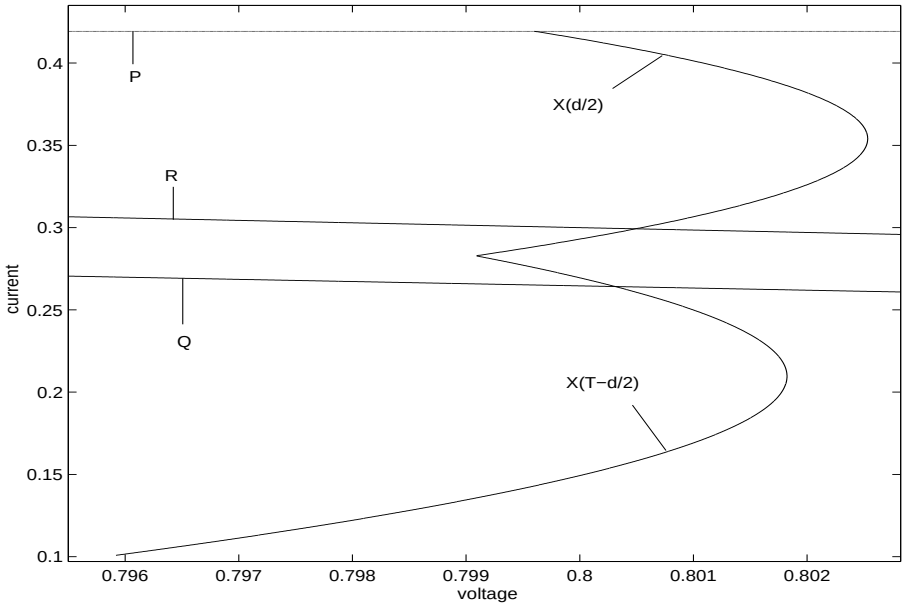

(b) k_s=0.5

Figure 3: Figure's author: Fabiola Angulo.

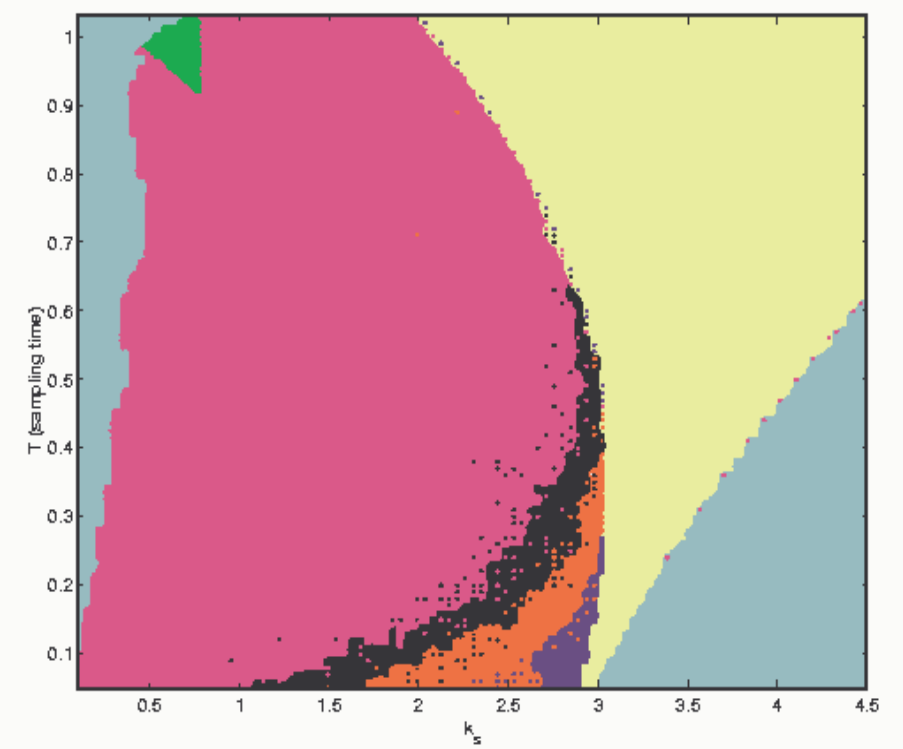

Figure 4: Figure's author: Fabiola Angulo.

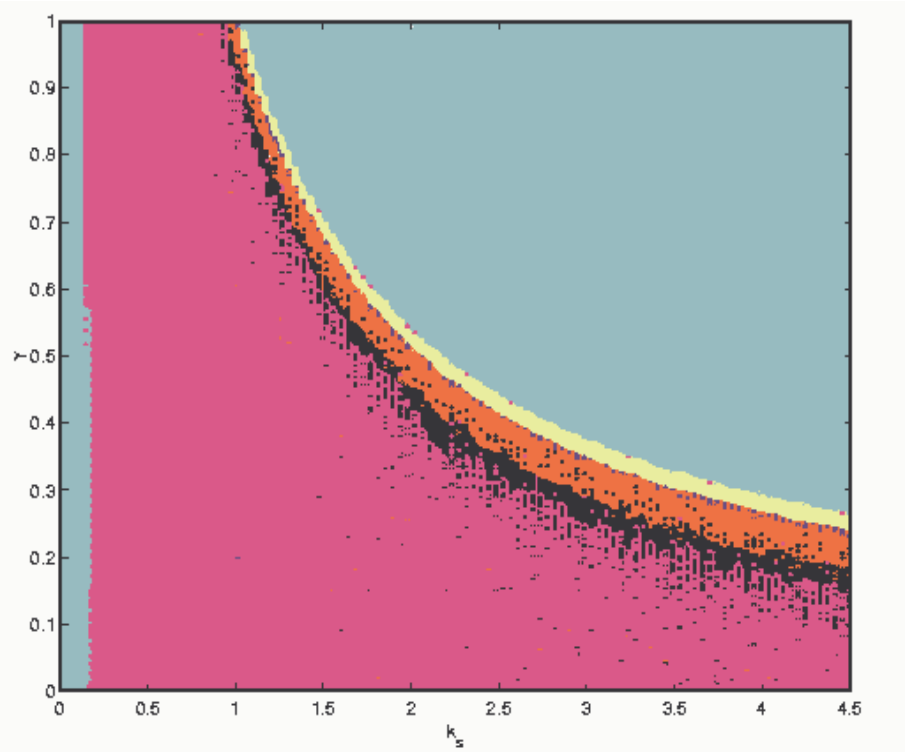

Figure 5: Figure's author: Fabiola Angulo.

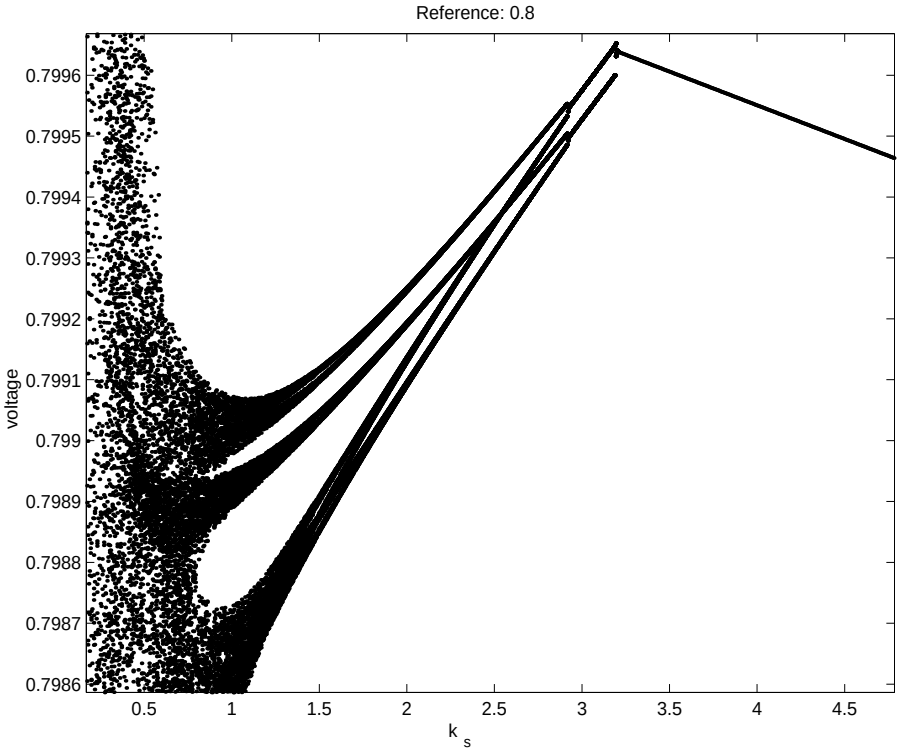

Figure 6: Figure's author: Fabiola Angulo.

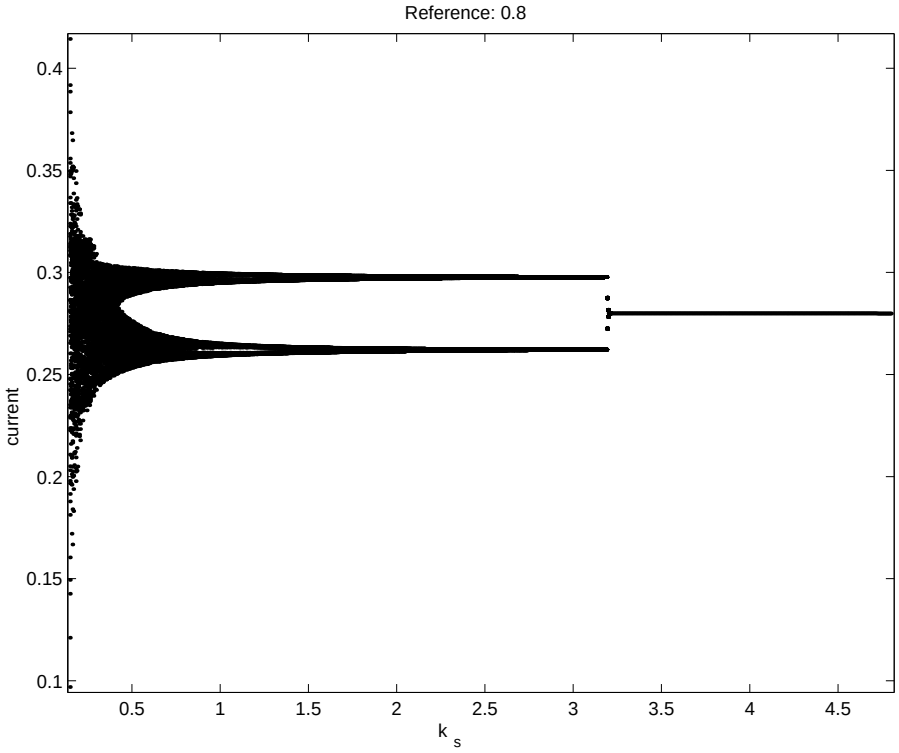

Figure 7: Figure's author: Fabiola Angulo.

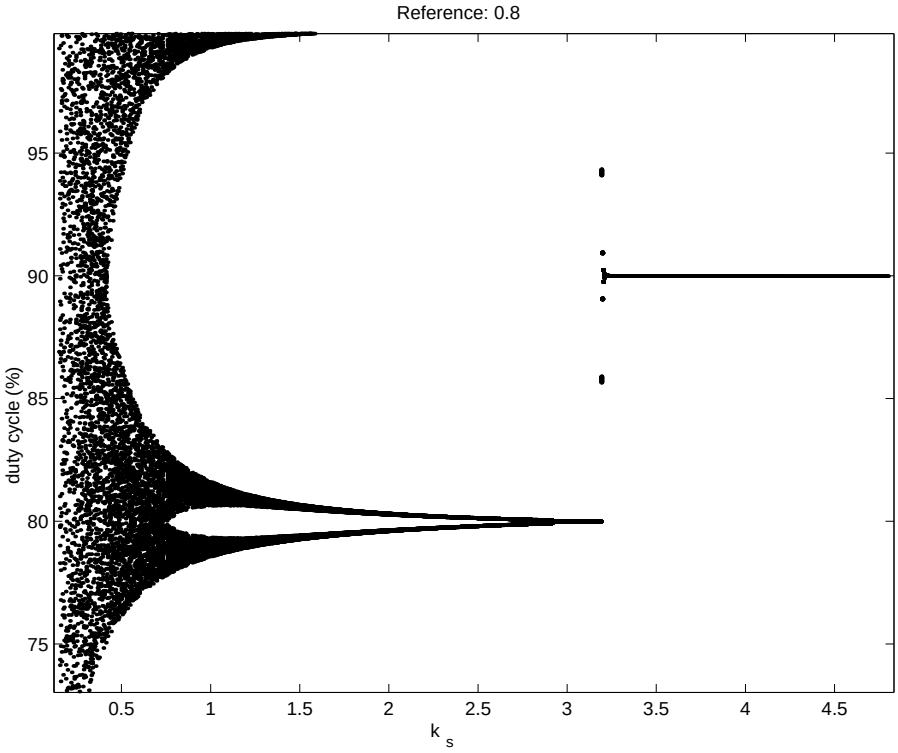

Figure 8: Figure's author: Fabiola Angulo.

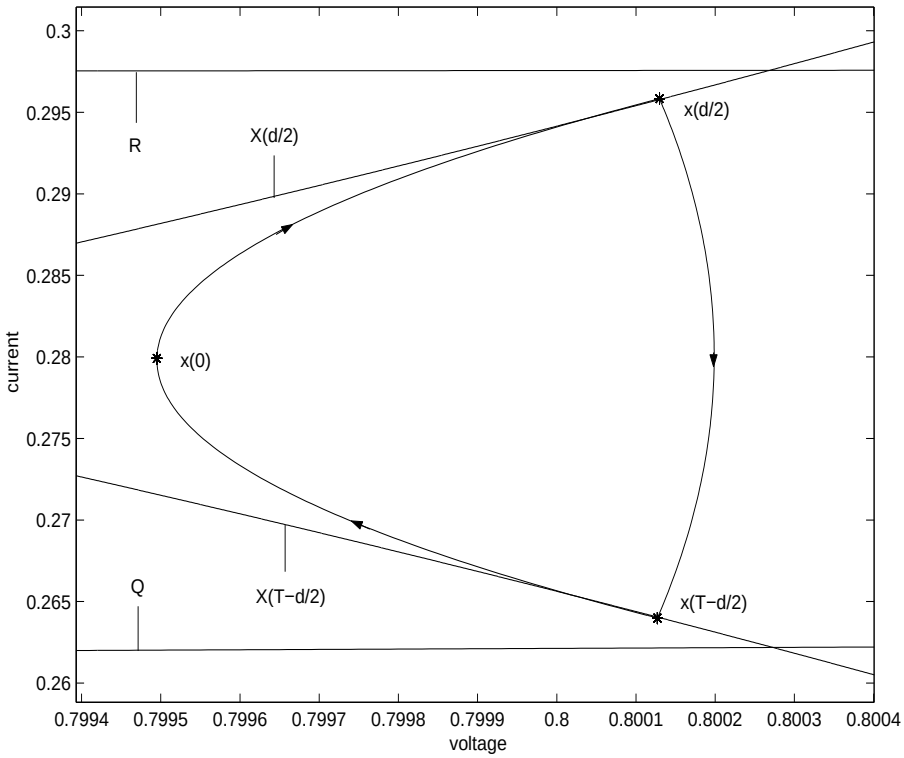

Figure 9: Figure's author: Fabiola Angulo.

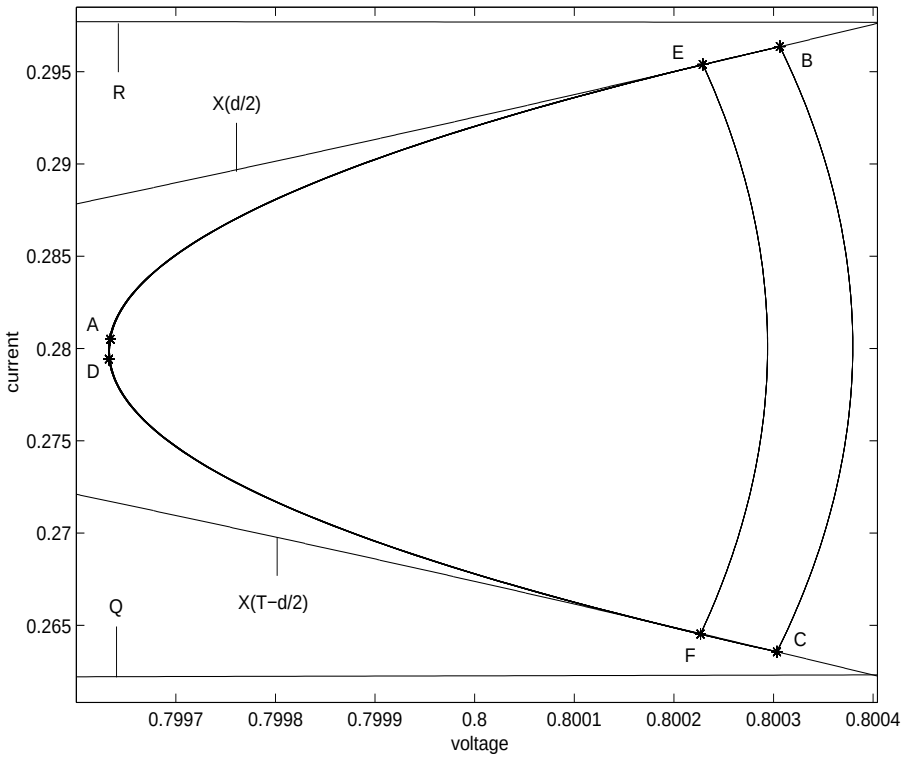

Figure 10: Figure's author: Fabiola Angulo.

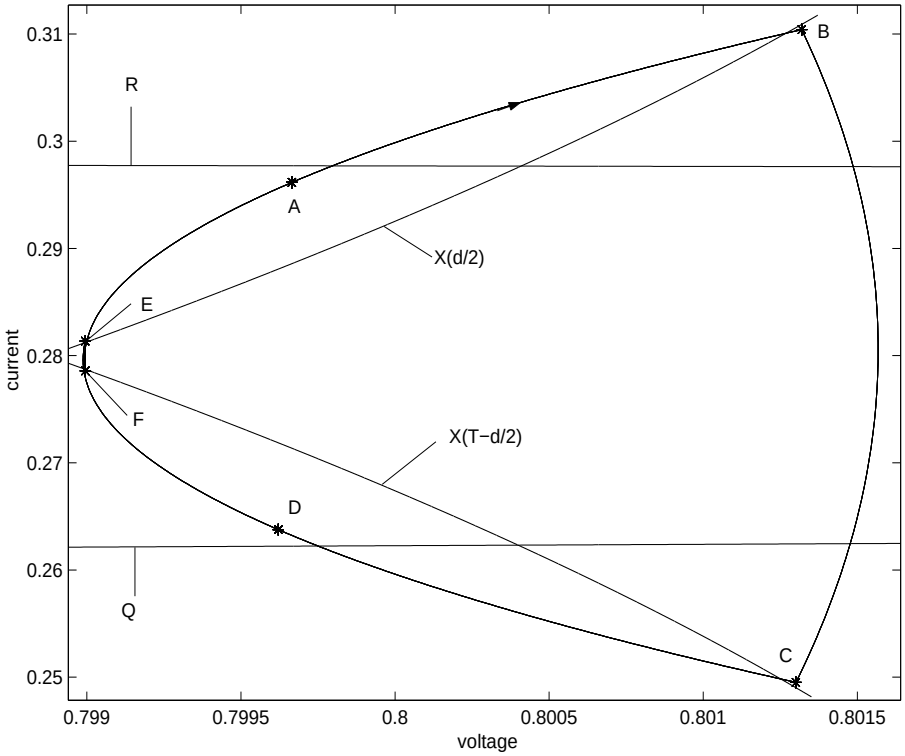

Figure 11: Figure's author: Fabiola Angulo.

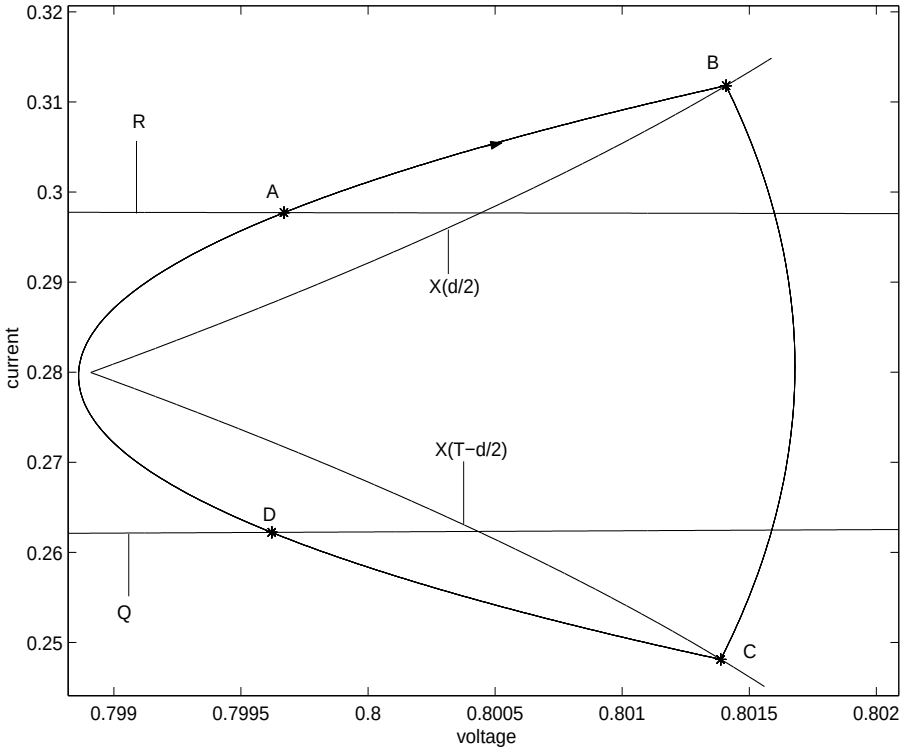

Figure 12: Figure's author: Fabiola Angulo.

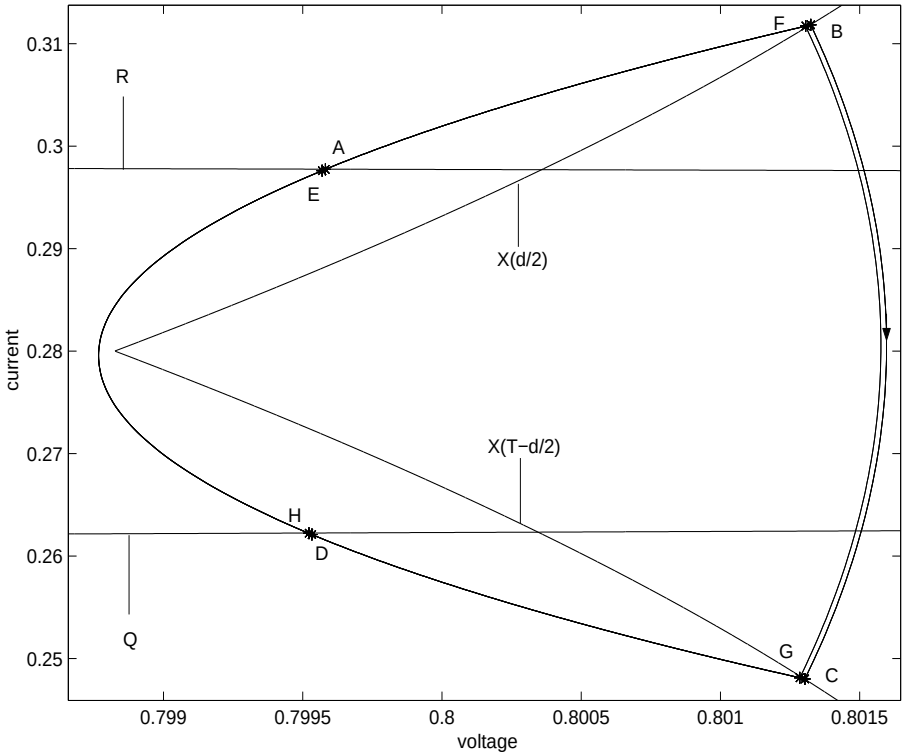

Figure 13: Figure's author: Fabiola Angulo.

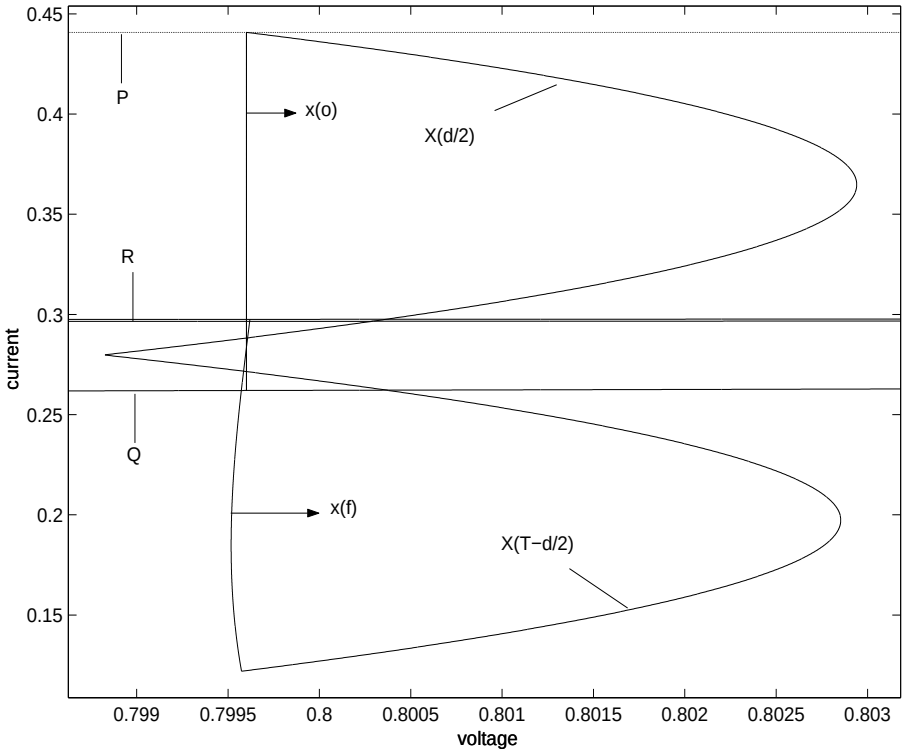

Figure 14: Figure's author: Fabiola Angulo.

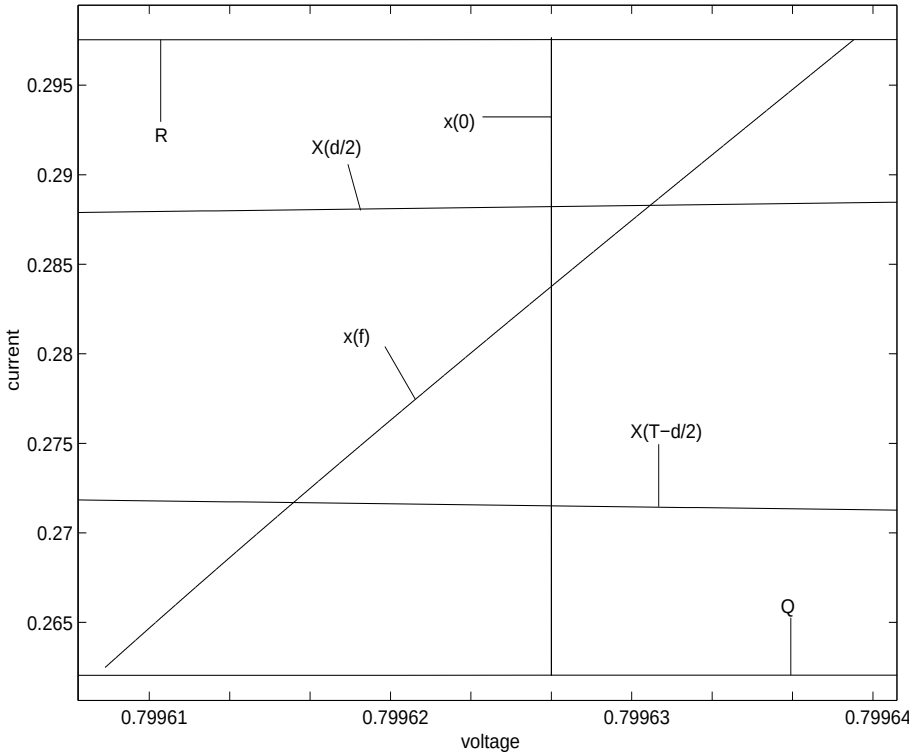

Figure 15: Figure's author: Fabiola Angulo.

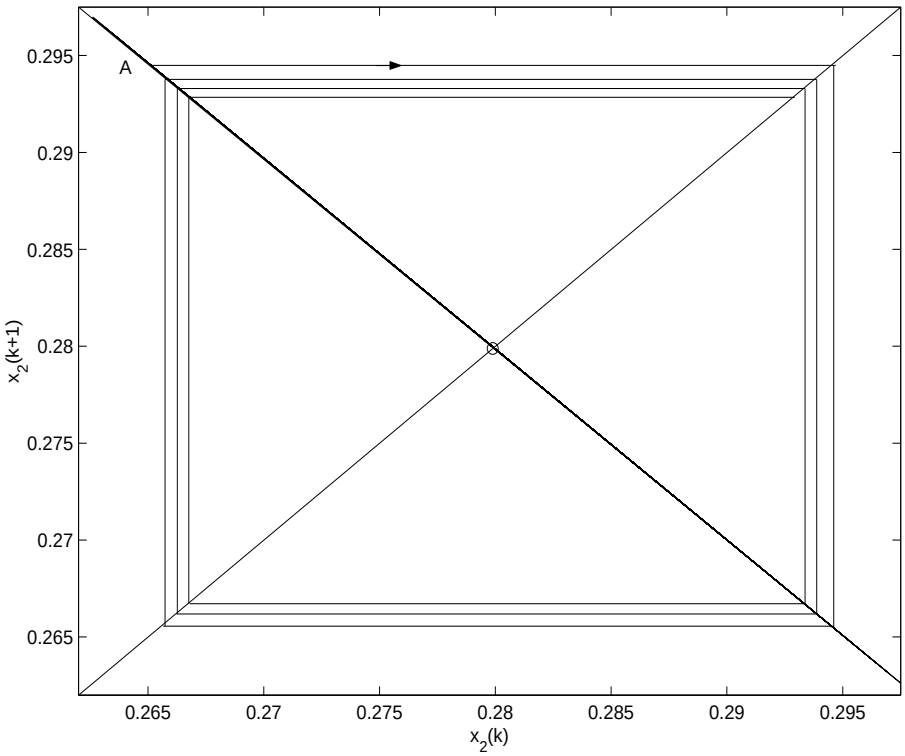

Figure 16: Figure's author: Fabiola Angulo.

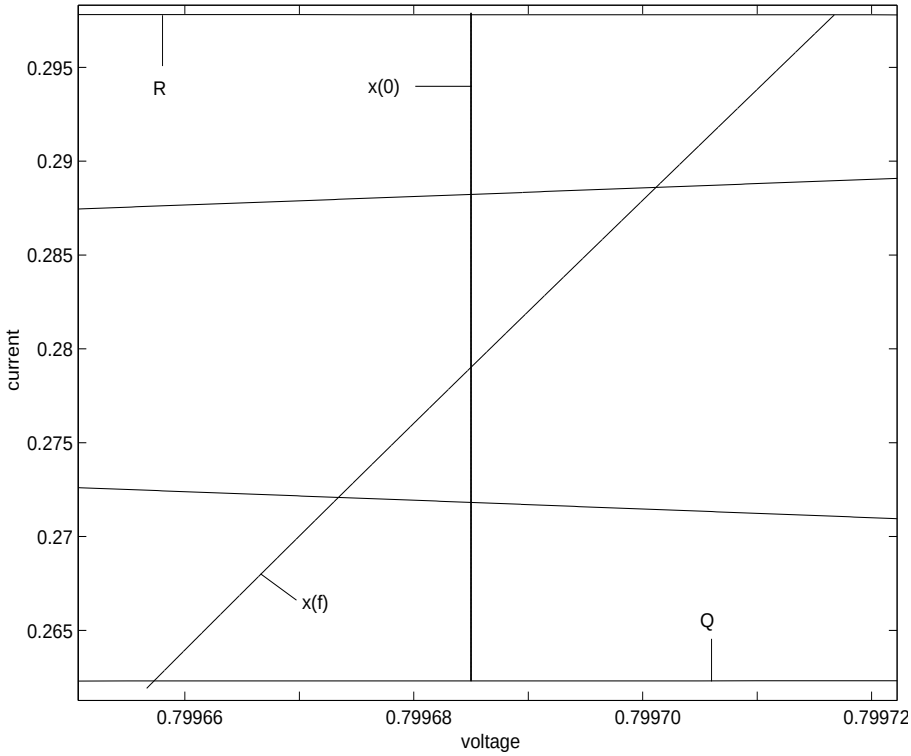

Figure 17: Figure's author: Fabiola Angulo.

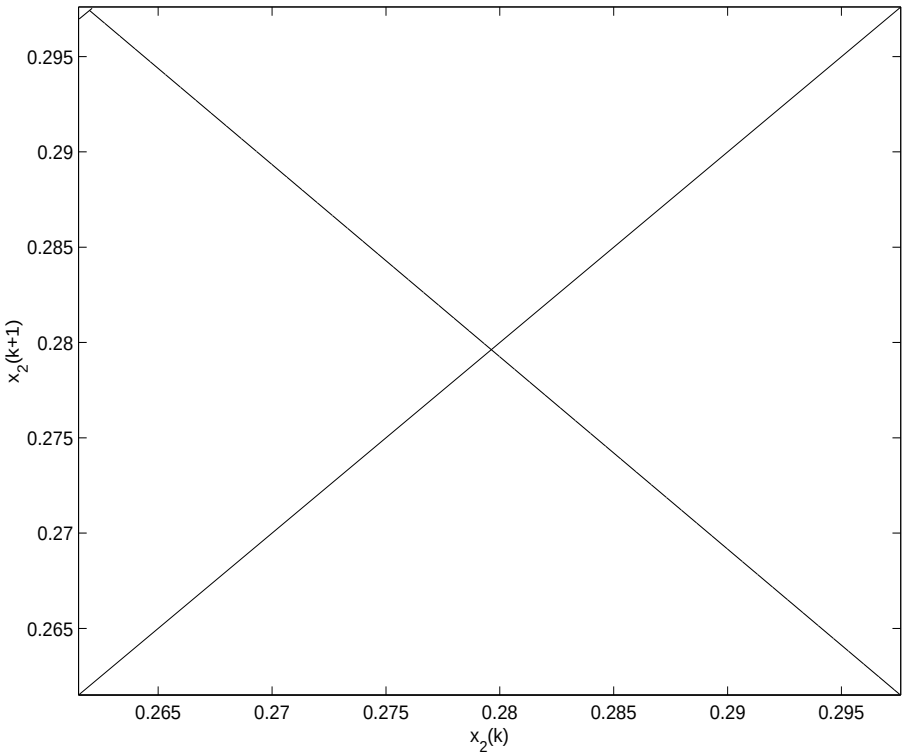

Figure 18: Figure's author: Fabiola Angulo.

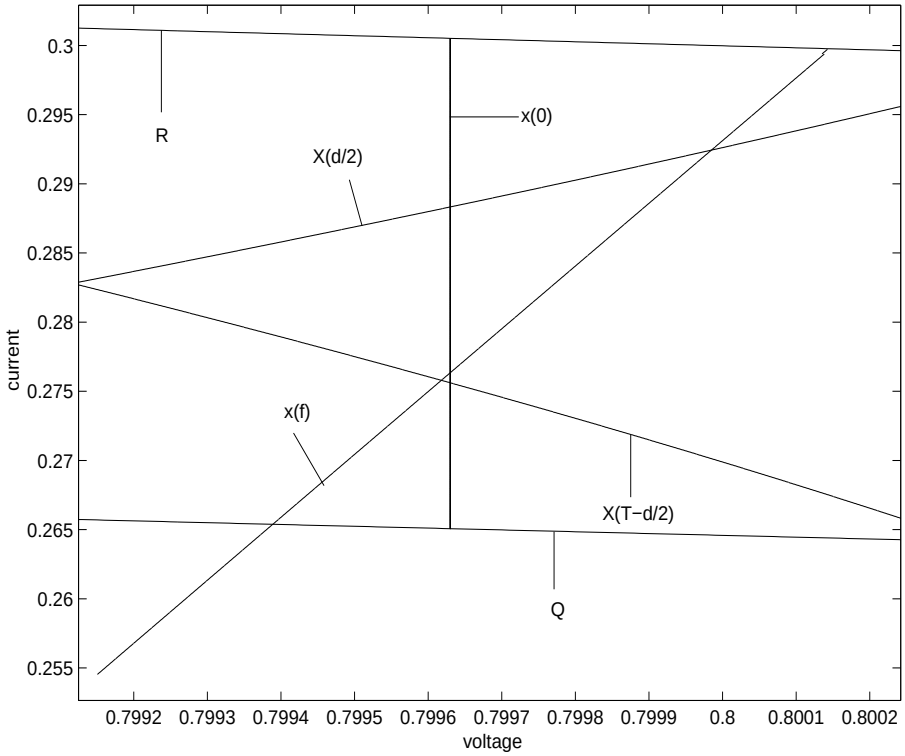

Figure 19: Figure's author: Fabiola Angulo.

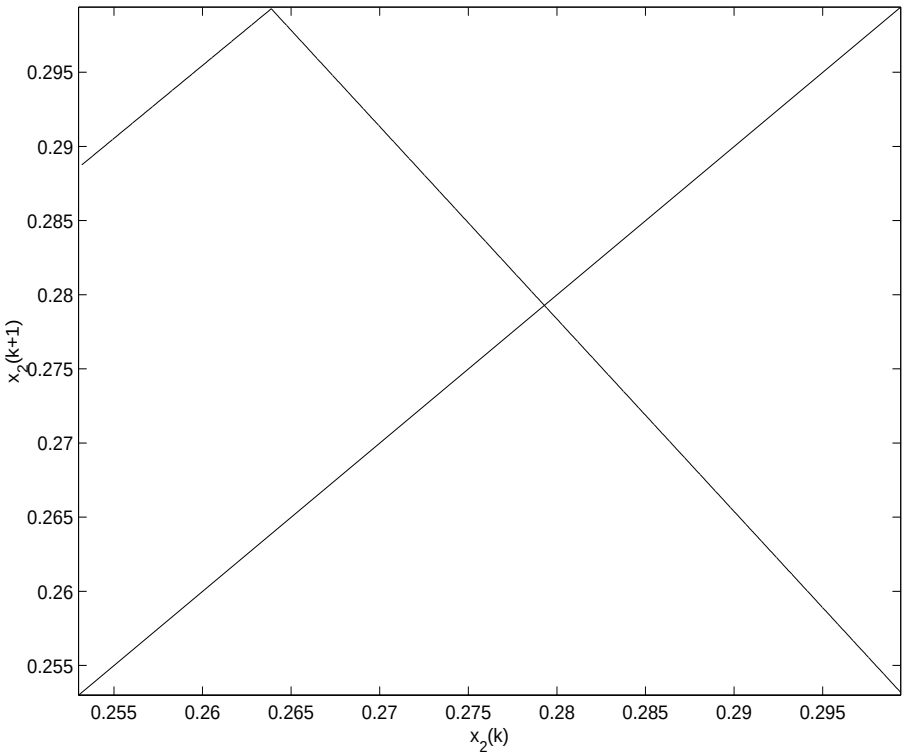

Figure 20: Figure's author: Fabiola Angulo.

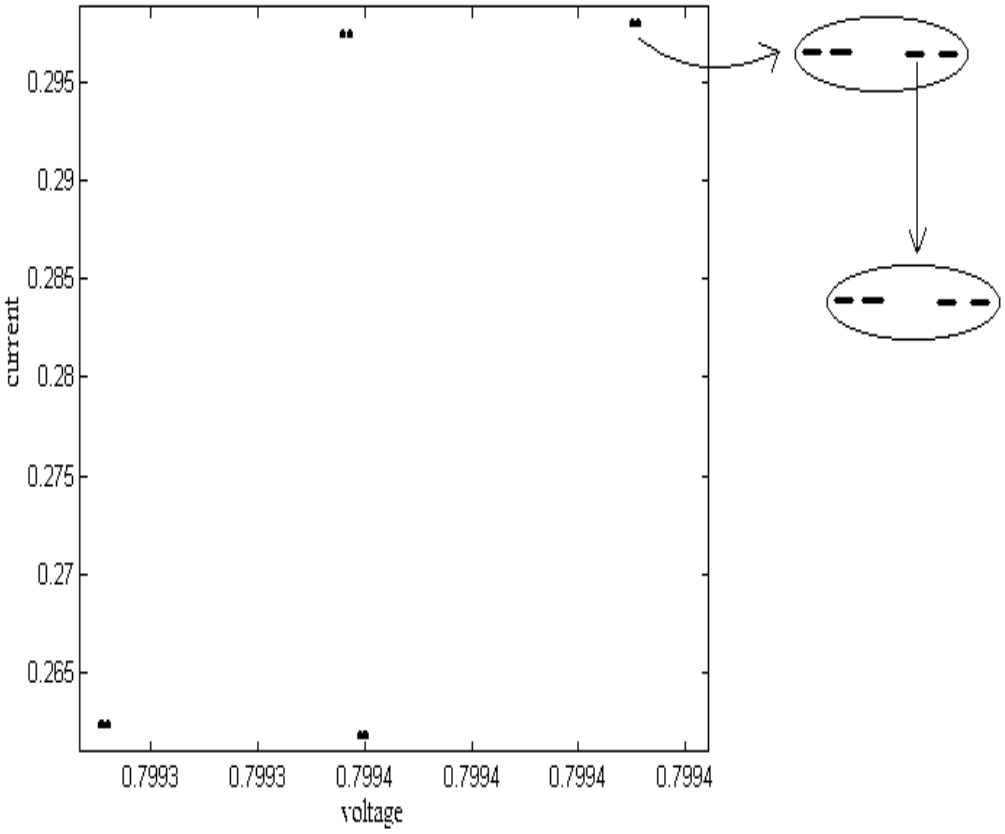

Figure 21: Figure's author: Fabiola Angulo.

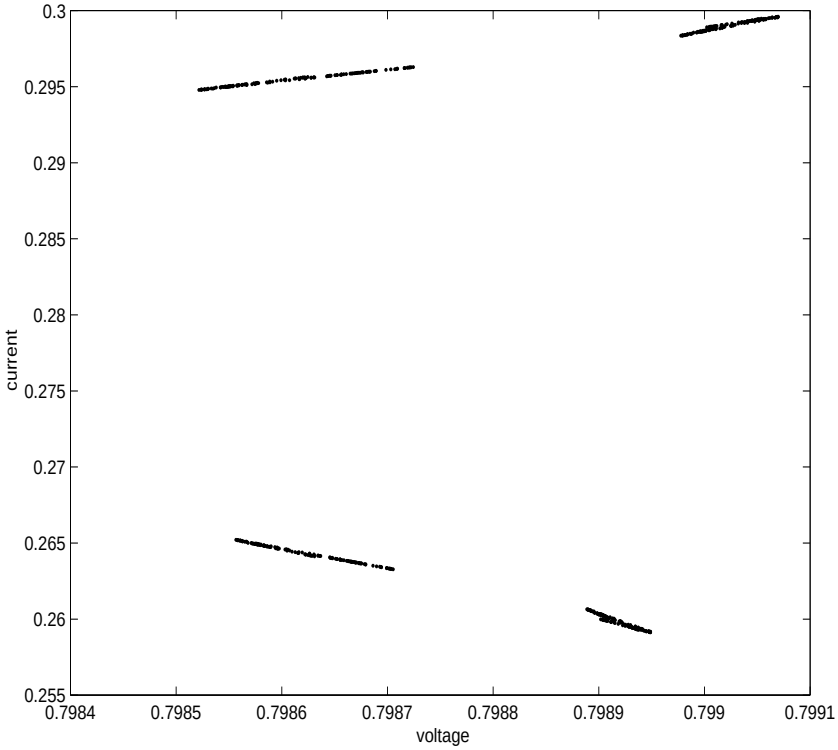

Figure 22: Figure's author: Fabiola Angulo.

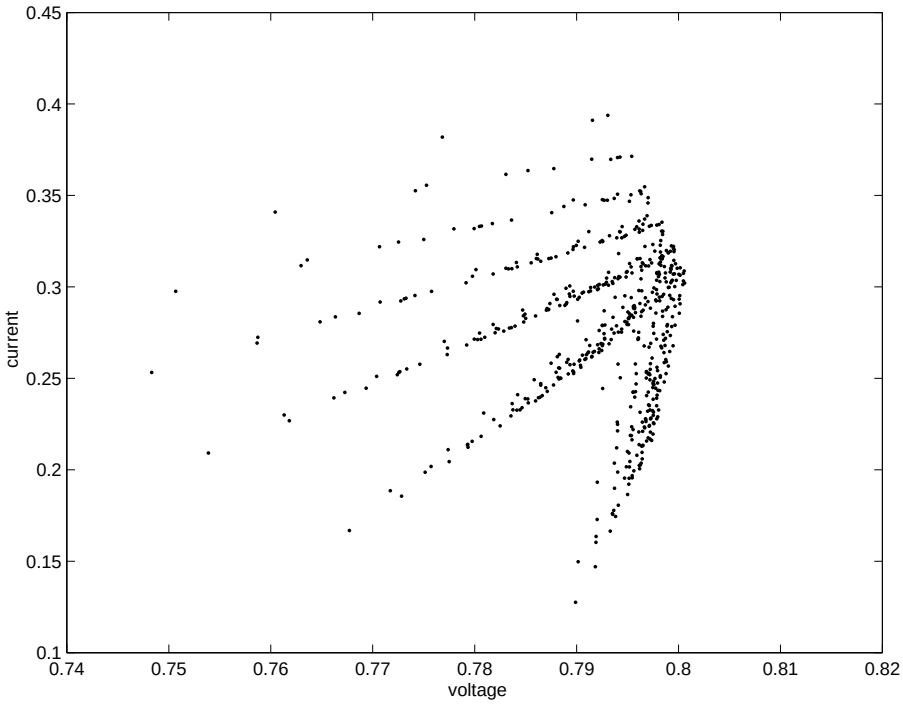

Figure 23: Figure's author: Fabiola Angulo.